JOURNAL OF GEOPHYSICAL RESEARCH, VOL. 102, NO. A5, PAGES 9603-9617, MAY 1, 1997

# HF-radar observations of the dayside magnetic merging rate: A Geospace Environment Modeling boundary layer campaign study

K. B. Baker
Applied Physics Laboratory, Johns Hopkins University, Laurel, Maryland

A. S. Rodger
British Antarctic Survey, Cambridge, England

G. Lu
High Altitude Observatory, National Center for Atmospheric Research, Boulder, Colorado

**Abstract.** Goose Bay HF-radar data have been used to determine the dayside reconnection electric field which transports energy from the solar wind into the Earth's magnetosphere and ionosphere. The speed of the ionospheric plasma flow perpendicular to the open/closed boundary is determined in the rest frame of the boundary along each of the 16 beam directions of the HF radar. The observations were made during one of the Geospace Environment Modeling program's boundary layer campaigns. The period from 1200 to 1600 UT on March 29, 1992, was one of generally southward interplanetary magnetic field (IMF). The $y$ component of the IMF was negative for most of the time. Despite the generally steady IMF conditions, the merging rate observed by the radar shows a great deal of temporal structure. The radar observations have been compared with the results from the assimilative mapping of ionospheric electrodynamics (AMIE) procedure. Initially, the merging inferred from the radar observations accounts for a significant portion of the total polar cap potential drop, suggesting that a majority of the potential drop was generated within the radar field of view and must therefore be due to magnetic merging at the magnetopause. At the end of the period, however, the potential drop derived from the radar measurements is distinctly less than that derived from the AMIE procedure. At that time, however, satellite and ground magnetometer data show that a substorm was in progress, and there is substantial evidence for a strong nightside contribution to the polar cap potential drop. An additional feature that appears in this data set is that the orientation of the open/closed magnetic field separatrix with respect to magnetic latitude is well correlated to the $y$ component of the IMF.

## 1. Introduction

One fundamental parameter required for accurate modeling of the energy flow in the coupled ionosphere-magnetosphere system is the time variation of the cross-polar-cap potential drop. Indeed, one of the major goals of the boundary layer campaign of the Geospace Environment Modeling (GEM) program is to measure the rate of magnetic merging along the dayside magnetopause as a function of time. There are several mechanisms that are involved with the generation of the polar cap potential, but during periods of southward interplanetary magnetic field (IMF) the process of magnetic merging along the dayside magnetopause is certainly one of the most important. The other major contribution occurs through reconnection in the geomagnetic tail, a process that often is seen episodically as part of the substorm process. A third element arises from processes known as viscous interactions, but these are thought to contribute only a small amount to the cross-polar-cap potential (a few kilovolts) during periods of southward IMF.

For southward IMF conditions, when solar wind magnetic field flux tubes merge with flux tubes connected to the Earth, ionospheric plasma which had been located on closed magnetic field lines finds itself on open field lines. The electric field drives the ionospheric plasma in the antisunward direction across the polar cap. The speed at which ionospheric plasma is transported across the open/closed boundary (hereafter referred to as the separatrix) provides a direct measure of the merging rate at the magnetopause. The dayside extent of the region where ionospheric plasma is transported from closed to open field lines is referred to as the merging gap.



Paper Number 97JA00288.
0148-0227/97/97JA-00288$09.00

The relationship between the local rate at which magnetic flux ($F$) is transported across a length $dl$ of the separatrix and the reconnection electric field ($E_{rec}$) is given by *de la Beaujardière et al.* [1991] as

$$dF/dt = \boldsymbol{B} \times \boldsymbol{v} \cdot \boldsymbol{dl} = E_{rec} dl$$

where $\boldsymbol{B}$ is the magnetic field at the separatrix and $v$ is the velocity of the plasma in the frame of reference of the separatrix.

The transport of plasma from closed to open field lines can take place either by the plasma convecting across a stationary boundary, or by the boundary moving equatorward across the plasma, or, in general, by both. The importance of knowing the motion of the separatrix as well as its orientation with respect to the plasma flow has been examined by *Lockwood et al.* [1988] and by *Lester et al.* [1990]. One of the first concentrated efforts to measure the reconnection electric field used data from the Sondrestrom incoherent scatter radar [*de la Beaujardière et al.*, 1991]. The measurements were made by performing elevation scans perpendicular to the Sondrestrom L shell. The operating assumptions for this approach were that the separatrix was oriented along the L shell and that the motion of the boundary could be described purely in terms of a change in magnetic latitude. The location of the separatrix was determined by the poleward boundary of the region of auroral electron precipitation.

The approach described here (section 2) has the distinct advantage in comparison with prior work that the orientation of the separatrix can be determined and the measurements are made across the entire field of view of the radar, a span of over 2 hours of magnetic local time (MLT), in as little as 96 s. The results (section 3) show that it is essential to know the orientation of the boundary, which can change substantially over relatively short time periods.

## 2. Data Sets and Methodology

### Interplanetary Magnetic Field

March 28–29, 1992, was the Sundial/Atlas 1 campaign period for which a number of studies have been or are being made [e.g., *Lu et al.*, 1996; *Szuszczewicz et al.*, 1996]. For the purposes of this study, however, the period was also selected as part of the boundary layer campaign for GEM. An additional reason for choosing the March 29, 1992, period was that the IMF conditions were relatively steady. Figure 1 shows the IMF and solar wind pressure in GSM coordinates for the period in question. No data from the IMP 8 satellite were available prior to 1320 UT. We note that the IMF $z$ component was negative for the entire interval, with a mean value around −5 nT, except for a brief period at ~1432 UT when it became slightly positive.

Initially, the $y$ component of the IMF was near zero, but just before 1400 UT there was a period of about 10 min when the IMF $B_y$ became positive. After 1400 UT, $B_y$ became more strongly negative and remained in a steady negative condition except for two very brief excursions to very small positive values at approximately 1430 and 1440 UT. The solar wind velocity, density, and the resulting dynamic pressure are shown in Figure 2. In general, the solar wind parameters were quite steady. Small spikes in the velocity can be seen at 1330, 1528, and 1550 UT, and a small spike in the density occurs at approximately 1415 UT. Except for the spike at 1415 UT, the dynamic pressure varied by less than 1 nPa during the nearly 3 hours from 1300–1600 UT.

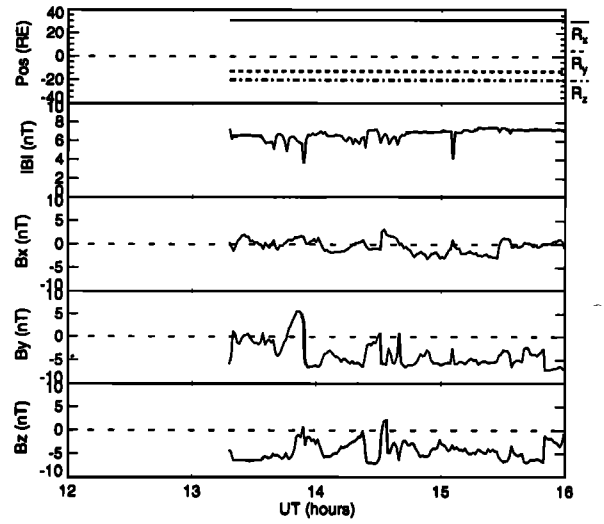


**Figure 1.** Interplanetary magnetic field (IMF) data from the IMP 8 satellite in GSM coordinates for March 29, 1992. The top panel shows the satellite position in Earth radii. The four lower panels show the magnitude and the three individual components of the IMF.

### Radar Data

The Goose Bay radar is a flexible coherent scatter HF radar, which scans over an azimuth sector of approximately 52° [*Greenwald et al.*, 1985]. The radar beam can be pointed in any one of 16 contiguous directions separated by approximately 3.3° in azimuth. During the period described here, the radar integrated on each beam position for 6 s. There was a small amount of overhead required to process the data so that the time step between successive beams is always slightly more than the integration period, and a full scan over all 16 beams typically required about 100 s. Along each beam, 70 contiguous range gates were sampled, each 30 km wide. The radar used a seven-pulse multipulse pattern to form a 17-lag autocorrelation function at each range gate. The derivation of the physical parameters such as the intensity of the backscattered power, the line-of-sight velocity, and the Doppler power spectral width is described by *Baker et al.* [1995].

In addition to the data from the Goose Bay radar, conjugate data from the Halley radar were also examined. The Polar Anglo-American Conjugate Experiment (PACE) is described in detail by *Baker et al.* [1989]. The purpose of the PACE experiment was to examine conjugate phenomena. Unfortunately, during the period of this GEM campaign, the backscattered signal observed by the Halley radar was weak, and it has not been possible to carry out the full analysis of the data with both radars.

Again, the day examined in this study, March 29, 1992, was one of the days chosen for the GEM boundary layer campaign, and the interval from 1200–1600 UT (corresponding to the time around MLT noon) was a period of

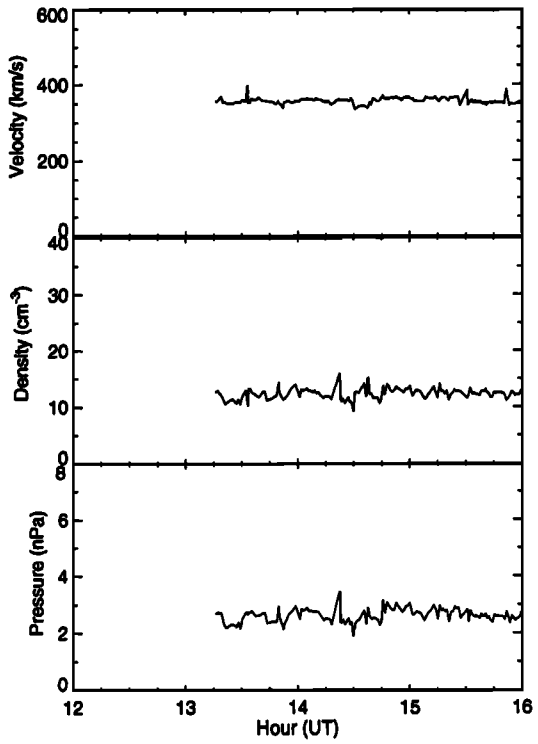


**Figure 2.** Solar wind parameters from the IMP 8 satellite. The top panel shows the bulk solar wind velocity in km/s, the middle panels shows the solar wind density in $cm^{-3}$, and the bottom panel shows the derived dynamic pressure in nPa.

good ionospheric backscatter for the Goose Bay radar. Plate 1 shows a time series plot of the radar data (backscattered power, line-of-sight velocity, and Doppler spectral width) along a single azimuth. It is interesting to note that the character of the radar backscatter shows a significant dropout which began at approximately 1352 UT. The radar data then begin to recover starting at about 1400 UT at the lower latitudes. The period from 1352–1400 UT corresponds to the period when the IMF $B_y$ was positive. Although the period of positive $B_y$ is brief, *Greenwald et al.* [1990] showed that the convection pattern clearly changes in response to the IMF $B_y$ variations on a timescale of less than 5 min.

Magnetic latitude in Plate 1 is given in the altitude adjusted corrected geomagnetic coordinate (AACGM) system, which is an updated version of the PACE geomagnetic coordinate system [*Baker and Wing,* 1989]. The software for implementing this coordinate system is publicly available, and further information on the AACGM system can be accessed via the World Wide Web at the uniform resource locator (URL) "http://sd-www.jhuap.edu/RADAR/AACGM.html."

The top panel of Plate 1 shows that there is a region of strong scatter that is seen almost continuously from 1225–1600 UT. The top panel also shows structures of particularly strong backscatter which propagate poleward during the period from 1400–1500 UT. The middle panel, showing the line-of-sight velocities, indicates that the region of strong backscatter is characterized by velocities away from the radar, that is, poleward-moving plasma.

The bottom panel is the estimate of the width of the Doppler power spectrum for the backscattering region. *Baker et al.* [1995] have demonstrated that the width of the Doppler power spectrum is an excellent diagnostic for locating the equatorward boundary of the ionospheric cusp. Specifically, they found that the equatorward edge of the region near noon where the spectral width exceeded 150 m/s was coincident with the ionospheric cusp as defined by the particle precipitation boundary described by *Newell and Meng* [1988], a result later confirmed by *Rodger et al.* [1995]. Using the spectral width criterion, the equatorward boundary of the cusp was located at approximately 75° magnetic latitude at 1225 UT and then showed a general equatorward motion over the next 4 hours, reaching a latitude of around 72° at the end of the period.

## Determination of the Convection Vectors

To determine the rate at which plasma flows across the separatrix, it is necessary to determine the two-dimensional plasma drift vectors. The technique described by *Ruohoniemi et al.* [1989] for determining the two-dimensional vectors from the line-of-sight velocities was used in this study. The errors which can result from this technique have been discussed by *Freeman et al.* [1991], but it should be noted that most of the time the results derived from the radar scans are in very good agreement with independent measurements of the velocity vectors. In particular, even though the cusp is a particularly dynamic region and contains flows which can vary significantly over the longitude range covered by the radar scan, the results of *Baker et al.* [1990] showed excellent agreement between the vectors obtained from the radar data and the plasma drifts measured by a simultaneous pass of the DMSP F9 satellite.

The technique for obtaining the two-dimensional vectors requires data over a moderate portion of the full radar scan. In addition, the technique provides the best results when the variations in the line-of-sight velocities are smooth functions of the radar azimuth. The line-of-sight velocity data were therefore averaged over three successive scans, resulting in two-dimensional vectors determined with a temporal resolution of approximately 5 min. Although this produced excellent vectors, it necessarily led to a loss of both spatial and temporal resolution. The impact of these losses in resolution will be considered in more detail in the discussion section.

## Determination of the Separatrix

The determination of the separatrix between open and closed magnetic field lines was made using a criterion based on the estimated spectral width of the Doppler power spectra [*Baker et al.,* 1995]. They showed that the equatorward edge of the region of large spectral widths is highly correlated with the equatorward edge of the particle precipitation region associated with the cusp [*Newell and Meng,* 1988, 1989; *Newell et al.,* 1989]. Recent work on the cusp and low-latitude boundary layer has suggested that the actual separatrix between open and closed magnetic field lines lies somewhat equatorward (~100–200 km) of the particle precipitation boundary [*Lockwood and Smith,* 1993; *Newell and Meng,* 1993, 1995]. However, since the flow patterns observed during this GEM cam-

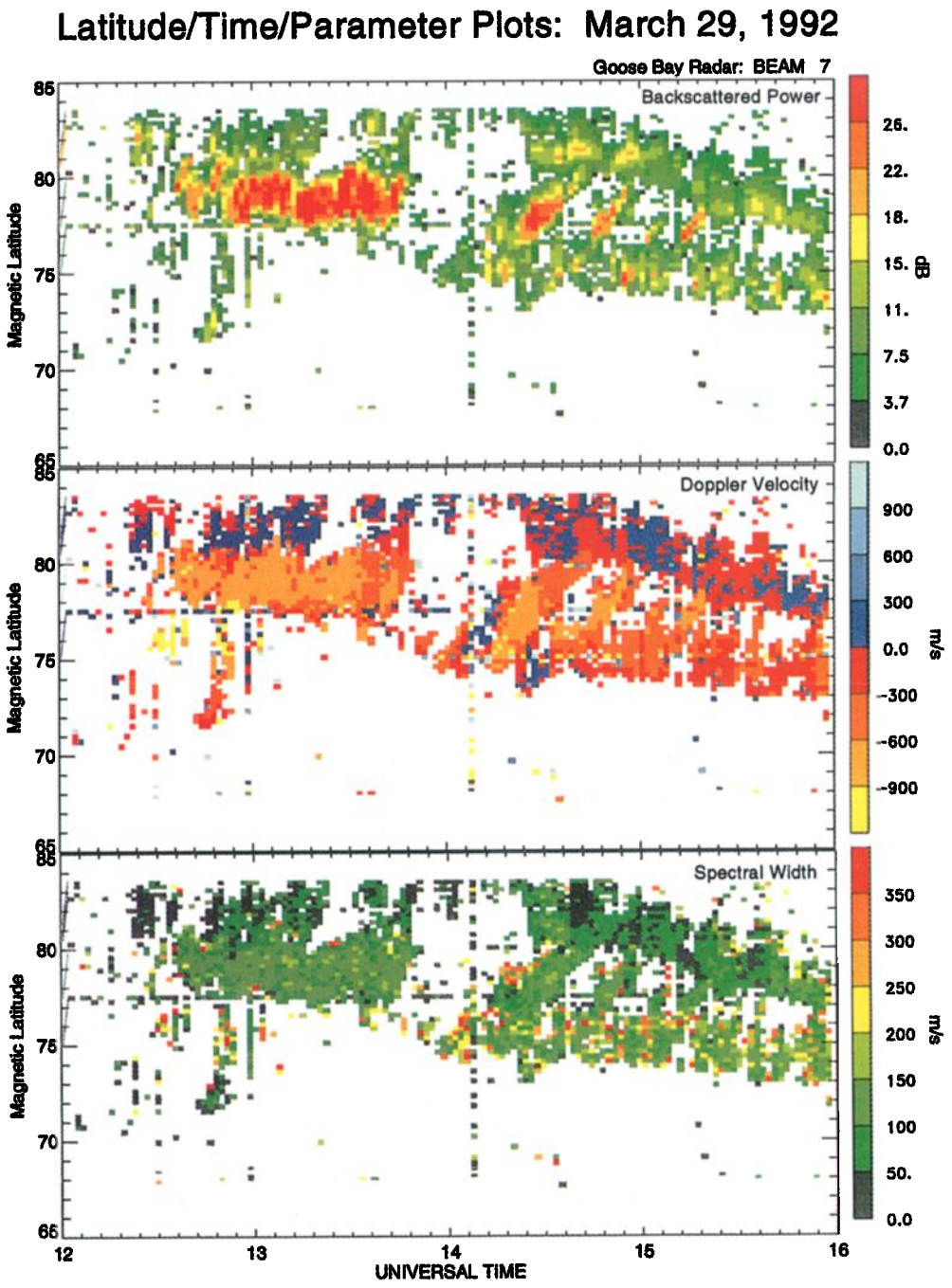


**Plate 1.** Time series plot showing the data from a single beam (beam 7) of the Goose Bay radar. In each panel, the time is indicated by the $x$ axis and the magnetic latitude of the observation point is given by the $y$ axis. The value of the parameter is indicated by the color. The top panel shows the intensity of the backscattered power in dB above the noise level. The middle panel shows the line-of-sight velocity, with red and yellow indicating motion away from the radar. The bottom panel shows the estimated width (full width at half maximum) of the Doppler power spectrum.

paign were relatively constant over 100 km around the boundary, a displacement of the true separatrix from that determined by the spectral width criterion will have little effect on the overall results.

Although there is a very strong correlation between the regions of high spectral width and the particle precipitation cusp, it is quite possible for an individual range gate in the radar data to either show an unusually large spectral width when normally the width would be narrow or vice versa. A complete understanding of the spectral features of the HF-radar data is not yet available, but certainly some of the anomalous spectra are due to noise from other transmitters, to extraneous backscattered power due to echoes from other ranges and other pulses of the radar, and to significant velocity shears occurring within a range-beam cell, as illustrated by *Pinnock et al.* [1995]. It is beyond

the scope of this paper to discuss these problems in any detail. To eliminate spurious shifts in the boundary due to these problems, the following technique was used. First, for each radar scan, the equatorward-most range gate with a spectral width greater than 150 m/s was located. Then a linear function of the magnetic latitude as a function of the magnetic longitude was fitted through the set of points. At least five points were required (i.e., a boundary point had to be determined on at least five beams of the scan). The resulting boundary could then be characterized by a simple function, giving the latitude at the center of the field of view and the orientation of the boundary with respect to the line of constant magnetic latitude.

Once these functions were determined, it was a simple matter to determine the motion of the boundary along any given radar beam. When dealing with the plasma flow across the separatrix, the location and orientation were smoothed with a running three-point (5-min) average in order to maintain consistency with the processing of the vectors. Although the fitting of the boundary points to a smooth curve has the disadvantage of eliminating any real small-scale variations of the boundary as a function of magnetic longitude, it made it possible to automate the task of calculating the plasma flow across the boundary. The implications of the loss of small-scale variations will be considered in the discussion.

### Determination of Plasma Flow Across the Separatrix

Once the two-dimensional flow vectors and location and orientation of the open/closed separatrix have been determined for each 5-min period, it is a straightforward matter to locate the vectors along the boundary and determine the component of the flow perpendicular to the boundary. The only complication comes in dealing with data gaps in the vector flows which may occur at the boundary. The ionospheric plasma is essentially incompressible (see, for example, the discussion of the ionospheric signature of flux transfer events, or FTEs, by *Southwood* [1987]), and in the absence of narrow field-aligned currents, which would lead to sharp velocity shears, we would expect the plasma flow across the separatrix to be relatively constant over distances of the order of 100 km. Examination of the observed flow patterns confirmed this expectation and therefore, when it was impossible to determine a vector exactly on the boundary, the nearest vector to the boundary was used, provided that it was within 100 km of the boundary. If no vector could be determined within a 100-km circle of the boundary point, then there was a gap in the determination of the flow. Again, the errors that might be expected from this will be considered in the discussion section.

## 3. Results

As an example of one 5-min period of this study, Figure 3 shows the flow vectors determined from the line-of-sight velocity data averaged over the period from 1437:31 to 1442:30 UT. The flow pattern is fairly uniform, and there are two distinct areas. The equatorward area shows flow velocities of the order of 600 m/s with a distinct poleward component to the flow. The velocities in the poleward region are similar in magnitude but are more L shell aligned. The jagged line which passes through the equatorward region of flow is the actual separatrix position (as determined by the spectral width) at each beam for the middle scan of the three that were incorporated into this 5-min average. The smooth curve through the region shows the fitted location and orientation of the separatrix. It is clear in this example that the flow vectors do not change appreciably over a 100-km range, so the exact position of the separatrix is not critical to the determination of the plasma flow across the boundary.

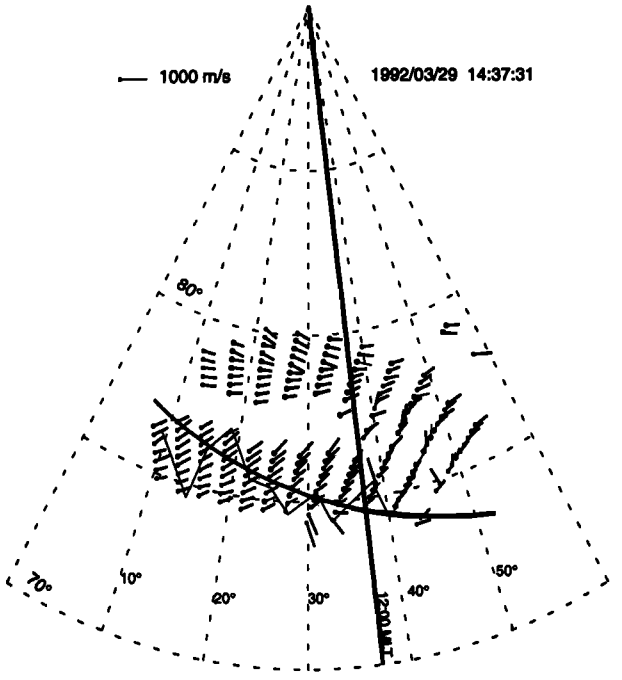


**Figure 3.** Plasma drift vectors derived from the Goose Bay radar data averaged over the period from 1437:31 to 1442:30 UT. The data are plotted in the altitude adjusted corrected geomagnetic coordinate system. The location of the most equatorward position on each beam where the spectral width exceeded 150 m/s is indicated by the jagged line crossing the field of view from west to east. The fitted position of the open/closed separatrix is indicated by the smooth curve.

The location and orientation of the boundary as a function of time is shown in Figure 4. The dashed lines indicate periods when the uncertainty in the location of the boundary was particularly high because the amount of radar backscatter was small. As noted earlier, there is a general trend of the separatrix from around 75° magnetic latitude at the start of the 4-hour period to about 72° latitude at the end.

The orientation of the boundary varies between about +10° to almost −40°, but most of the time it is around −10° to −20° (a positive rotation is counterclockwise with respect to the L shell). Although there appears to be an oscillation in the orientation of the boundary with a period of around 10 min, a Fourier analysis of the data does not show any well-defined frequency. The orientation of the boundary with respect to the lines of constant magnetic latitude is generally from the northwest to the southeast. The exceptions to this occur during the earliest part of the interval of the study when no IMF data are available and

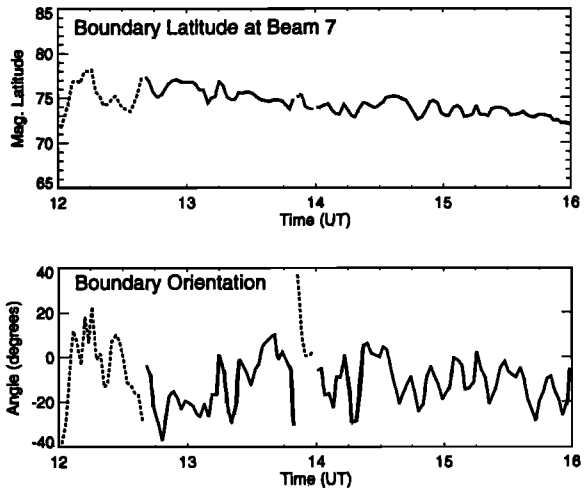


**Figure 4.** Location and orientation of the open/closed separatrix. (top) The magnetic latitude of the separatrix on beam 7. (bottom) The orientation of the boundary with respect to a line of constant magnetic latitude. Negative angles indicate a boundary which runs from the northwest to the southeast.

in the period around 1400 UT when the $z$ component of the IMF is small and $B_y$ is briefly positive.

A comparison of the boundary orientation with the IMF suggests that the orientation of the separatrix becomes steeper (more negative) as the $y$ component of the IMF becomes more negative. In order to test this, a correlation of the IMF and the boundary orientation was performed. A simple correlation of the 5-min data shows only a very weak correlation (a maximum of 0.34 for the correlation with $B_y$). However, the quasi-periodic behavior of the separatrix orientation does not appear to be reflected in the IMF data. A more appropriate measure of the correlation between the boundary orientation might therefore be found for longer-period variations. In order to examine that possibility, the data for the boundary orientation and the IMF were both filtered with a low-pass digital filter with a cutoff period at 15 min. To avoid problems with the end points of the filter, the cross correlation was restricted to the period from 1330 to 1530 UT for the IMF data. The boundary orientation was then correlated with the IMF data using a sequence of lags of the boundary orientation with respect to the IMF. The results are shown in Figure 5. The strongest correlation (0.72) occurs when the boundary orientation lags the IMF $B_y$ by 1.8 min. This correlation is significant at the >>99.9% level. There is also a correlation between IMF $B_x$ and the boundary, but this relationship is unphysical, as the orientation changes well before the IMF (>5 min).

The correlations between the boundary angle and both the ratio $B_y/B_x$ and the angle $\tan^{-1}(B_y/B_x)$ were also examined, but in both cases the correlations were much lower than for either IMF component alone. On first impression, the 1.8-min lag seems quite short, given that the satellite was about 30 $R_E$ upstream of the Earth (~20 $R_E$ upstream of the magnetopause), and several minutes of delay might be expected between the solar wind observations and the ionospheric response. However, the spacecraft was also about 20 $R_E$ below the ecliptic plane. It is quite possible with this geometry for the IMF variations to encounter the magnetopause before they are observed at the IMP 8 satellite.

Once the magnetic field variations encounter the magnetopause, the ionospheric response near noon can be very rapid. *Clauer and Banks* [1986] used the Sondrestrom incoherent scatter radar to examine the response of the ionospheric convection pattern to IMF $B_z$ variations and found that the ionospheric response occurred on timescales of less than 15 min. Several other studies have been carried out using the European Incoherent Scatter (EISCAT) radar and found even quicker response times. *Willis et al.* [1986] reported a clear example when the ionospheric response to a $B_z$ change at the magnetopause required only 4 min. Similar results have been found by *Etemadi et al.* [1988] and *Todd et al.* [1988]. The conjugate study by *Greenwald et al.* [1990] suggested that the response of the ionospheric convection pattern to changes in the $y$ component of the IMF may be even more rapid. Further support for the near simultaneity of the IMP 8 observations and the ionospheric response is provide by the timing of the disappearance and reappearance of ionospheric scatter just prior to 1400 UT as noted earlier.

It is of some interest to attempt to make the relationship between the IMF $B_y$ component and the separatrix orientation more quantitative, but it must be emphasized that this is a case study for a limited period of time and cannot be taken as a valid statistical determination of a relationship between IMF and the separatrix orientation. Figure 6 shows a scatter plot of the IMF $B_y$ values versus the corresponding boundary orientation angles. Note that we have taken the boundary orientation angle as measured at a lag of 1.8 min after the IMF values. Note also that there actually appear to be two populations of points, a group with IMF values running from about $-6$ nT to about $-2$ nT and a second group clustered between about $-1.75$ nT and 0 nT. If we perform a linear regression on the total collection of points, we obtain the thin line for the regression, which is given by the equation

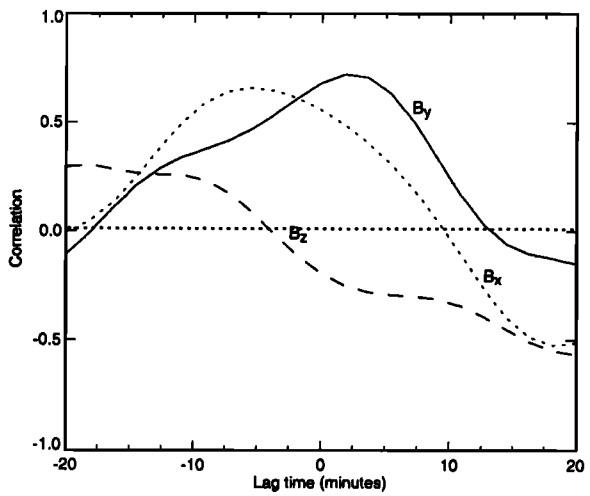


**Figure 5.** Cross correlation of the IMF (B) with the separatrix orientation angle (q). The solid line shows the correlation with $B_y$, while the dotted and dashed lines show the correlations with $B_x$ and $B_z$, respectively. The maximum correlation coefficient (0.72) occurs for $B_y$ with the boundary angle lagging the IMF by 1.8 min.

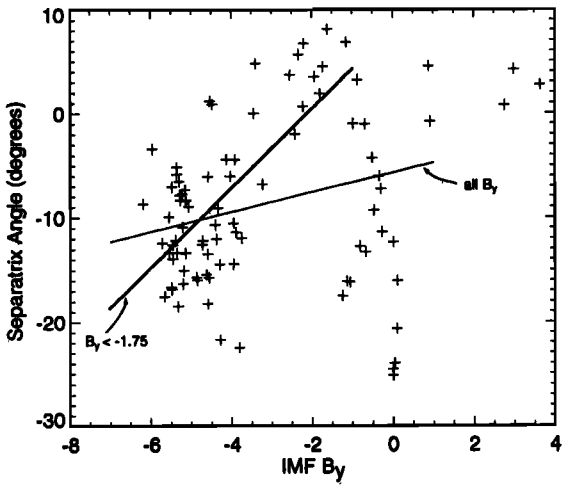


**Figure 6.** Scatter plot of the separatrix orientation angle versus the IMF $B_y$ value. The orientation angle was determined at a lag of 1.8 min. after the $B_y$ measurement. The thin solid line shows the regression line determined from using all the points, while the thick solid line shows the regression obtained from only those points where $B_y < -1.75$ nT.

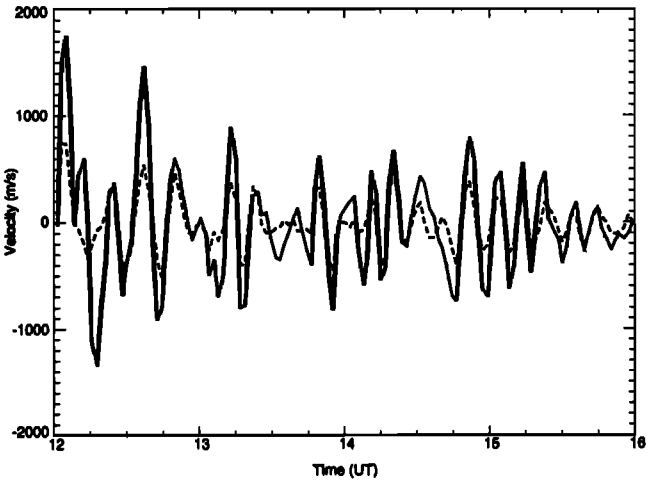


**Figure 7.** Motion of the separatrix versus time (UT) along beam 7 of the radar. The motion in the direction of the magnetic meridian is shown by the solid line, while the motion along the L shell is shown by the dashed line. Positive values are toward the pole and toward the east.

$\theta = -5.7 + 0.94\,B_y$. However, if we restrict the regression to the points with $B_y < -1.75$ nT, we get a much steeper relationship, $\theta = 8.0 + 3.8\,B_y$.

The solar wind velocity, density, and pressure (see Figure 2) appear to be uncorrelated either with the IMF or with the boundary latitude and orientation. Although we would normally expect a correlation of the separatrix position with respect to the solar wind dynamic pressure, in this case the dynamic pressure is relatively constant and the variations in the separatrix position and orientation appear to be controlled by the IMF variations. The correlation between the IMF and the pressure at zero lag was a low 0.09, and the maximum in the cross correlation between the boundary orientation and the pressure was 0.35 at a lag of −10 min.

The motion of the separatrix both perpendicular and parallel to the magnetic meridian is shown in Figure 7. The meridian component is usually larger than the zonal component and can be comparable to the plasma velocity. Both components show oscillatory behavior with a period of about 10 min.

An example of the resulting plasma flow across the separatrix is shown in Figure 8. Here the plasma flow is presented for beam 7, which is one of the central beams and is oriented slightly to the east of magnetic meridian. The dotted line shows the flow in the Earth's reference frame, while the dashed line shows the motion of the boundary that must be added to the flow to obtain the flow in the reference frame of the moving separatrix. The net result is indicated by the solid line. The gaps are due to periods when no vectors within 100 km of the boundary could be located. Although the motion of the separatrix can sometimes be quite fast, the addition of the boundary motion is usually not a very significant correction to the plasma flow. However, around 1300 UT, the contribution due to the boundary motion is around 20% of the total. Similar results were found for all the beams, reflecting the generally well-organized nature of the flow patterns. Unfortunately there are no IMF data for the period prior to 1315 UT, when the boundary motion is making its greatest contribution to the flow.

Once the velocity across the separatrix is determined in the reference frame of the boundary, the reconnection electric field in the ionosphere is determined by multiplying the flow velocity by the magnitude of the magnetic field. Figure 9 shows the reconnection electric field for each of the 16 beams of the radar. As might be expected from the flow pattern shown in Figure 3, the reconnection electric field exhibits a great deal of similarity from one beam to the next. The final step in the analysis is to integrate the reconnection electric field along the separatrix to determine the potential drop within the radar field of view as a function of time. For regions where the reconnection electric

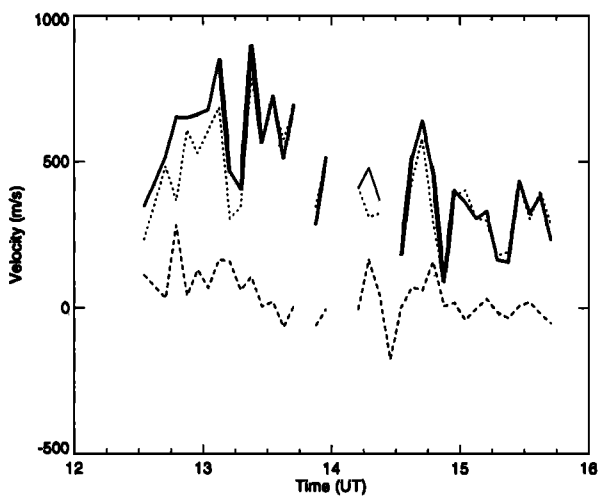


**Figure 8.** Velocity of the plasma flow perpendicular to the separatrix on beam 7 of the radar. The dotted line shows the flow speed in the Earth's rest frame. The dashed line shows the correction to the speed that must be made to convert to the rest frame of the separatrix. The resulting plasma flow speed in the separatrix frame is shown by the solid line.

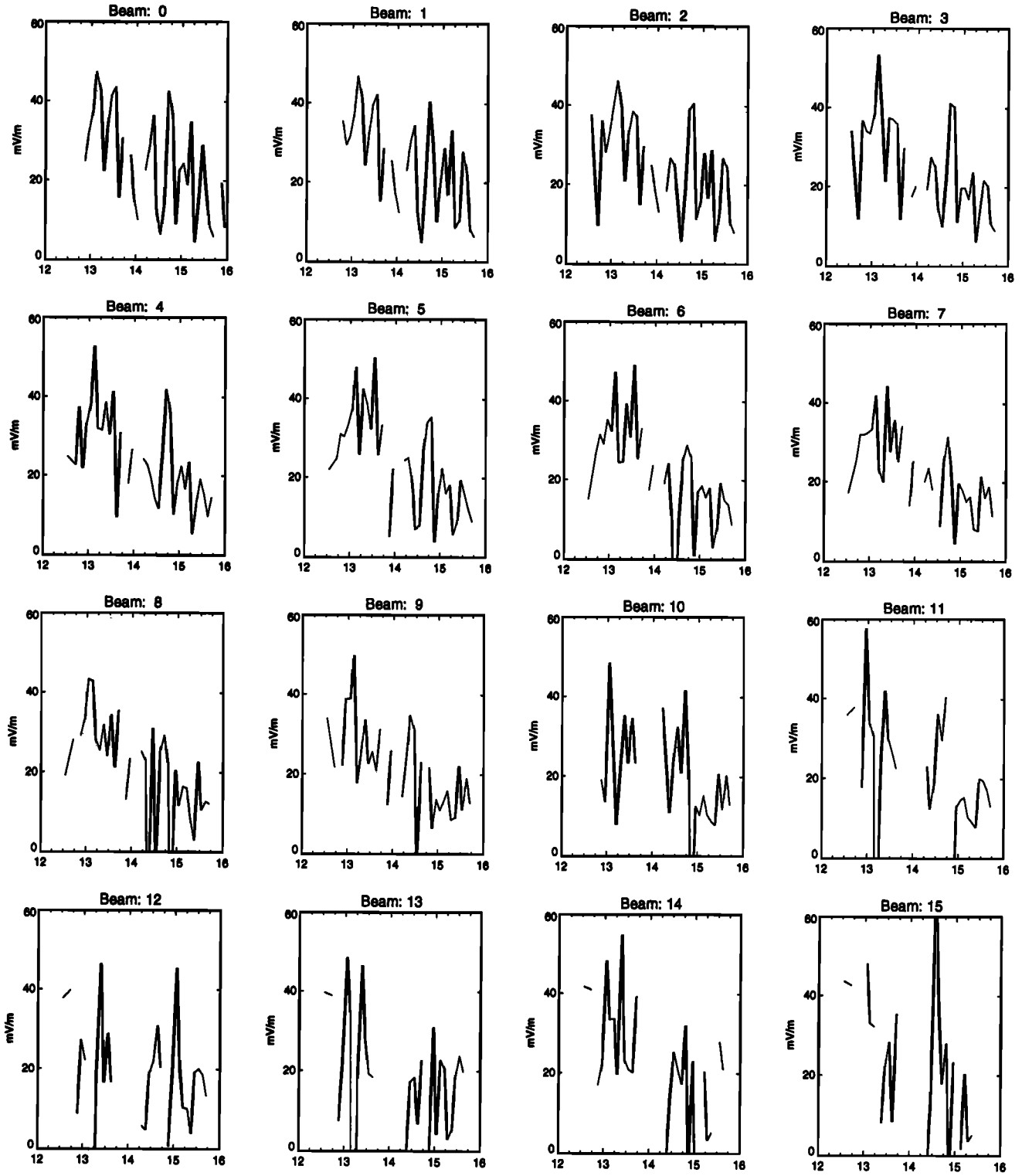


**Figure 9.** The reconnection electric field as a function of time (UT) is shown for each radar beam. Gaps indicate that a flow vector could not be found within 100 km of the separatrix on that beam.

field could not be determined, a simple linear interpolation through the missing points has been used. The results are shown in Figure 10. The dashed portions of the curve indicate the periods when the potential is likely to be seriously in error, either because there were only a few points with radar backscatter along the separatrix or because the separatrix itself was not well determined. The symbols indicate the number of points along the separatrix where the electric field was determined (diamond, 13–16 points; plus, 9–12 points; asterisk, fewer than 9 points). Before 1345 UT, the mean potential drop determined from the radar data is around 40 kV. At 1410 UT, the observed potential drop is only about 25 kV, and it then shows a generally decreasing trend, ending with a value of about 10 kV at

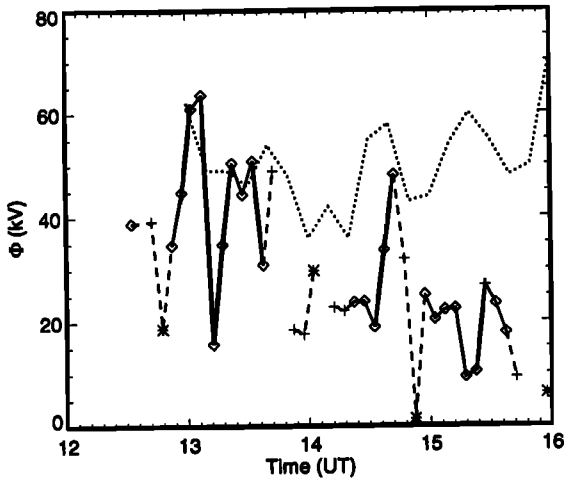


**Figure 10.** The potential drop along the separatrix as a function of time is shown by the solid and dashed line. The dashed portions indicate periods when the reliability of the radar data is poor, because of lack of radar backscatter along the separatrix. The individual points are marked with symbols to indicate the number of points at which radar backscatter was observed along the separatrix. The diamonds indicate 13–16 points, the plus signs indicate 9–12 points, and the asterisks indicate fewer than 9 points. The dotted line shows the polar cap potential derived from the AMIE procedure.

1600 UT.

In recent years the assimilative mapping of ionospheric electrodynamics (AMIE) technique [*Richmond and Kamide,* 1988; *Richmond* 1992] has been widely used in a number of investigations [e.g., *Richmond et al.,* 1988; *Emery et al.,* 1990; *Knipp et al.,* 1991, 1993; *Lu et al.,* 1994] to examine the polar cap potential and ionospheric convection patterns. The AMIE model has been applied to the period of this study by *Lu et al.* [1996] to characterize the global convection pattern, and the polar cap potential derived from this technique has also been plotted in Figure 10. For this study, AMIE used over 100 data sets from magnetometers, DMSP ion driftmeters, and coherent radars, as well as data from the Goose Bay radar. Although the AMIE patterns are therefore not completely independent of the Goose Bay radar data, the changes produced by eliminating the Goose Bay data from the AMIE runs result in relatively small variations in the total potential drop across the polar cap. For example, the AMIE potential drop at 1500 UT was determined to be 44 kV when the Goose Bay radar data were included in the calculation and 43 kV when excluded. The largest difference was found for the potentials calculated for 1600 UT. When the radar data were included, the potential drop was 71 kV compared to 77 kV when the radar data were excluded, a difference that is still less than 10%. During the initial period of this study, the AMIE results are quite consistent with the radar results, but during the latter half of the period, the radar results give a polar cap potential drop of less than half the AMIE value. A more detailed analysis of the comparison of the radar and AMIE results will be left to the discussion section.

## 4. Discussion

### Uncertainties and Errors

The approach adopted in this study provides the first effort at describing the reconnection electric field over an extended longitude in the ionosphere. The technique suffers from some uncertainties arising from the determination of the separatrix and the flow across it. Some assessment of these uncertainties and the underlying assumptions are discussed in this section.

The method used here requires a smooth boundary to avoid introducing errors caused simply by noise in the radar signal. *Lockwood et al.* [1993] have found that there are occasions when the separatrix boundary jumps equatorward with no plasma motion and then moves poleward with equal plasma flow. In the frame of reference of the separatrix, this would mean an initial burst of poleward plasma flow (and hence magnetic flux) across the separatrix, followed by a period when there was no plasma flow across the separatrix. *Pinnock et al.* [1995] found a case where flow bursts appeared to originate equatorward of the separatrix boundary, which maintained a relatively steady position, and the plasma convected rapidly across this stationary boundary. In the frame of reference of the boundary, these two situations are in fact quite similar. Periods of rapid flow across the boundary were followed by periods when the flow across the boundary was smaller.

The question that must be addressed in the context of this study is, how much net flux might be crossing the real separatrix boundary as a result of equatorward and poleward fluctuations in the latitude of the boundary over small longitudinal distances? Figure 3 gives a good estimate for the magnitude of the errors that might occur due to localized fluctuations in the boundary. By comparing these fluctuations from one 96-s scan to the next, we estimate that a localized change in the boundary of about ±2° in latitude over a longitudinal region of 200 km might occur. If these fluctuations are true motions of the separatrix, then the amount of flux which can be added (or subtracted) would be of the order of $2 \times 10^6$ webers over a time period of a single scan (100 s), resulting in a voltage of 20 kV. Thus a sudden localized expansion in the position of the separatrix could provide a very significant contribution to the potential.

However, the fluctuations we have observed in the separatrix indicate that over the longitudinal sector covered by the radar scan, there are approximately as many poleward fluctuations as there are equatorward ones. Thus, if (as we suspect) the real boundary is relatively smooth and most of the small-scale variations around the smooth boundary are, in fact, due to noise in the radar signal, then the flux added to the polar cap is very small. Alternatively, if all these small-scale variations are real variations in the boundary and, at the same time, each equatorward fluctuation results in rapid flow of plasma across the boundary (i.e., the picture given by *Lockwood et al.* [1993]), then the flux that would be added to the polar cap during the formation of the bulge would result in an additional 20 kV to the voltage.

In the picture given by Lockwood et al., the bulge relaxes back to the main boundary, and during that time there is no flow across the boundary of the bulge. In the calculations presented here, there is continued flow across the smooth boundary, and thus the net magnetic flux that is added to the polar cap will be about the same as in the Lockwood picture. The difference is that in the Lockwood

et al. picture all the flux is added during a very brief period, so that a voltage spike is produced, whereas in the calculations presented here the voltage spike would be smoothed out over the 5-min integration period.

One source of uncertainty in the results presented here is related to the method of determining the two-dimensional flow vectors. The primary problem in this context is not the uncertainties discussed by *Freeman et al.* [1991], which are related to the longitudinal changes in the flow, but rather the temporal variability. The method used here was designed to maximize the number of vectors that could be obtained. This necessitated an average over three radar scans to generate one vector map. The initial step in the method described by *Ruohoniemi et al.* [1989] involves a least squares fit of the line-of-sight velocities along an L shell to a cosine law. When doing this fit, points which are far from the curve are discarded, and the remaining points are refitted. A localized burst of flow will therefore tend to be discarded. Thus, while steady flows are usually determined very successfully by this method, localized variations in the velocity on short timescales are not. Note, however, that bursts of high-speed flow, which cover a large portion of the region of ionospheric backscatter and last for a period comparable to one scan (100 s), will be properly incorporated into the 5-min averages, and in that case the average flow determined by this method should be a good indication of the average reconnection electric field for that period. By looking at high time resolution line-of-sight data from the PACE radars for other events [see, e.g., *Pinnock et al.*, 1995], the uncertainties in the velocities are estimated to be of the order of $\pm 200$ m/s over a region of 200–300 km along the separatrix. In terms of the potential that is derived from these data, the resulting error would be around 3 kV.

High time resolution studies of the cusp using the Halley radar have [*Pinnock et al.*, 1995] suggested the possibility that patchy (i.e., spatially localized) merging may result in brief, narrow equatorward extensions of the separatrix boundary. In addition, their results suggest the possibility that several independent events may occur simultaneously at more than one site on the magnetopause. However that interpretation has been challenged by *Lockwood and Davis* [1997] who suggested that the observed signature could be the result of intermittent reconnection at a single site. In this work, the analysis technique, which utilizes the full scan information, does not require any assumption concerning the longitudinal extent of an FTE.

## Temporal and Spatial Resolution of the HF-Radar Measurements

The technique used to estimate the velocity vectors ignores patches of high-speed flow that do not cover a significant segment along an L shell. Thus contributions to the polar cap potential that are generated by patches of merging whose ionospheric footprint are less than about 400 km in longitudinal extent will be missed by this analysis, and this is true no matter how long such a localized patch of merging might last. However, if a small patch of merging resulted in the separatrix moving equatorward, that effect would be observed by the radar.

Similarly, brief bursts of merging on timescales less than a single scan would only be picked up by the radar on a few beam directions, even if the burst covers a large spatial area. These brief bursts would be indistinguishable from a small patch of merging, and as in the patchy merging case, such brief bursts of merging would be missed by this analysis.

However, if a burst of merging covers more than 400 km in longitudinal extent and lasts for more than about 1 min, the 5-min average flow vectors would include the effect of the flow burst. If a relatively steady sequence of such bursts occurs with the time between bursts being less than 5 min (the time average used here), then they would be indistinguishable from steady merging and would be considered to be quasi-steady. If such bursts are separated by more than 10 min, we would expect to see a sudden enhancement in the resulting potential drop whenever they did occur, followed by a return to a lower value immediately after. The situation is more ambiguous if such bursts occur on timescales between 5 and 10 min, or if bursts occur even faster than 5 min but have large variations in magnitude. An examination of Figure 10 shows that the potential drop over the radar field of view can vary by over 20 kV from one 5-min period to the next, indicating that bursts of merging are occurring on timescales of less than 10 min. Our data sampling and analysis methods do not allow us to be more specific about the time distribution of FTEs.

## Comparison of the AMIE Results With the Radar Measurements

The *Kp* values for the period 1200–1600 UT on March 29, 1992, were 3– and 4–. Under these conditions, we would expect the cross-polar-cap potential drop to be around 60–90 kV [*Heppner and Maynard*, 1987]. The potential drops measured by the radar reach a maximum of just under 60 kV around 1300 UT, but the average for the period from 1240–1340 UT is around 40 kV. Later, when the *Kp* index increases, the potential determined from the radar actually decreases. Although the potential derived from the radar data seems to be low, detailed modeling using the AMIE technique indicates that the actual potentials tended to be lower than what might be expected from the *Kp* values.

Figure 11 shows the potential contours derived from the AMIE procedure at 1300, 1400, 1500, and 1600 UT. In each case the data used as input for the AMIE procedure were averaged over a 10-min period centered on the hour. The field of view of the radar is also shown in each plot. If nearly all the cross-polar-cap potential drop is being generated by merging on the dayside, then nearly all the contours would have to pass through the merging gap. The AMIE results would then indicate that the merging gap actually occupies about half the total polar cap boundary. There are two alternatives: (1) about half the polar cap potential drop is actually being generated by nightside reconnection, or (2) the rather coarse grid used by the AMIE procedure when coupled with the tendency of mag-

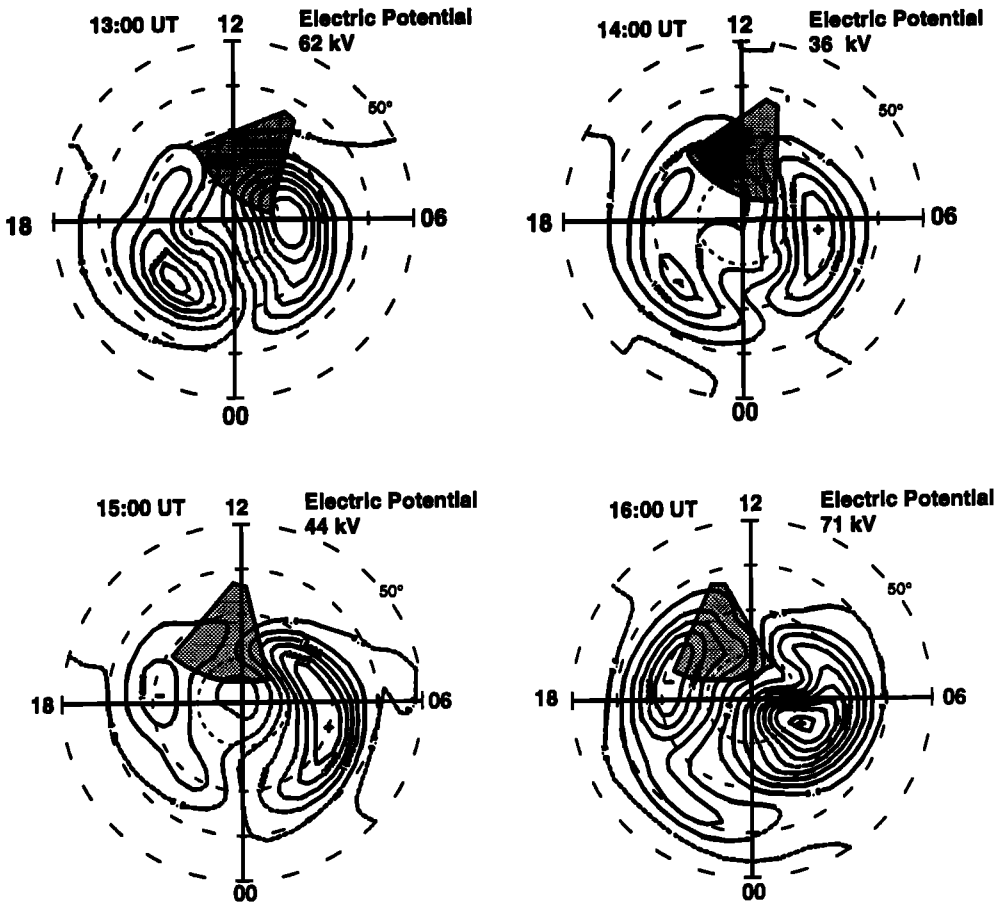


**Figure 11.** AMIE plots for the 10-min periods around 1300, 1400, 1500, and 1600 UT. The field of view of the Goose Bay radar is indicated by the shaded wedge in each plot.

netometer data to integrate over distances of about 200 km results in potential contours which are more spread out than is actually the case. The alternatives are not mutually exclusive, and undoubtedly, both effects are present. As can be seen in Figure 11, many of the contours are outside the radar field of view. If the contours are accurate in position, this would indicate that the radar should see only about half the total AMIE potential. This is the case for the period after 1400 UT, but before that the radar-derived potentials are very close to the AMIE values. This strongly suggests that the potential contours should be crowded into a smaller dayside merging gap.

The only really anomalous results come from the 1600 UT map, when the radar data showed a very low potential drop and the AMIE results indicated a steeply increasing potential. As Figure 9 indicates, at 1600 UT, there were gaps in the determination of $E_{rec}$ on most of the beams. Since the points where the reconnection electric field was measured showed rather low values, the interpolation and extrapolation of these points to cover the field of view would likely result in a low value of the total potential drop. Nevertheless, an examination of the electric field values just prior to 1600 UT suggests that the potential determined by the radar would have remained low even if reliable measurements had been available on all beams. The AMIE contours for this period indicate that about half the contours are inside the radar field of view.

An examination of particle data from the Los Alamos geosynchronous satellites is shown in Figure 12. A clear particle injection signature is seen at approximately 1515 UT. The *AE* index is shown in Figure 13, and the response of the electrojets to the substorm particle injection is clearly visible, with the maximum being reached at about 1600 UT. The details of the AMIE contours are strongly determined by the conductivity model used. A substorm is apt to produce large variations in the auroral conductivities, and it is therefore quite likely that the smooth AMIE contours for this period do not accurately reflect the true structure of the polar cap potential. The AMIE and radar data are entirely consistent with the idea that an important driver of convection at 1600 UT is reconnection in the tail and that the dayside merging rate only provides a small portion of the potential drop.

## Separatrix Orientation

If one assumes the antiparallel merging model [e.g., *Crooker*, 1979] it is clear that the IMF $B_y$ will cause the merging line on the magnetopause to be tilted with respect to the magnetic equator. This would have no direct effect on the orientation of the separatrix in the ionospheric, however, since the mapping of the field line from the magnetopause to the ionosphere is quite independent of the position of the merging point on that field line.

If the merging rate across the magnetopause is not the same, it might be possible for the merging on one side (the dusk side for example) to proceed faster than on the other side. Presumably, after some period of steady IMF and solar wind dynamic pressure, the magnetopause would reach a nonsymmetric equilibrium position. A tilt in the ionospheric separatrix would be the direct result. *Roelof and Sibeck* [1993] have investigated the shape of the magnetopause as a function of IMF $B_z$ and solar wind dynamic pressure, but to our knowledge, no one has extended that work to include effects due to $B_y$ or $B_x$.

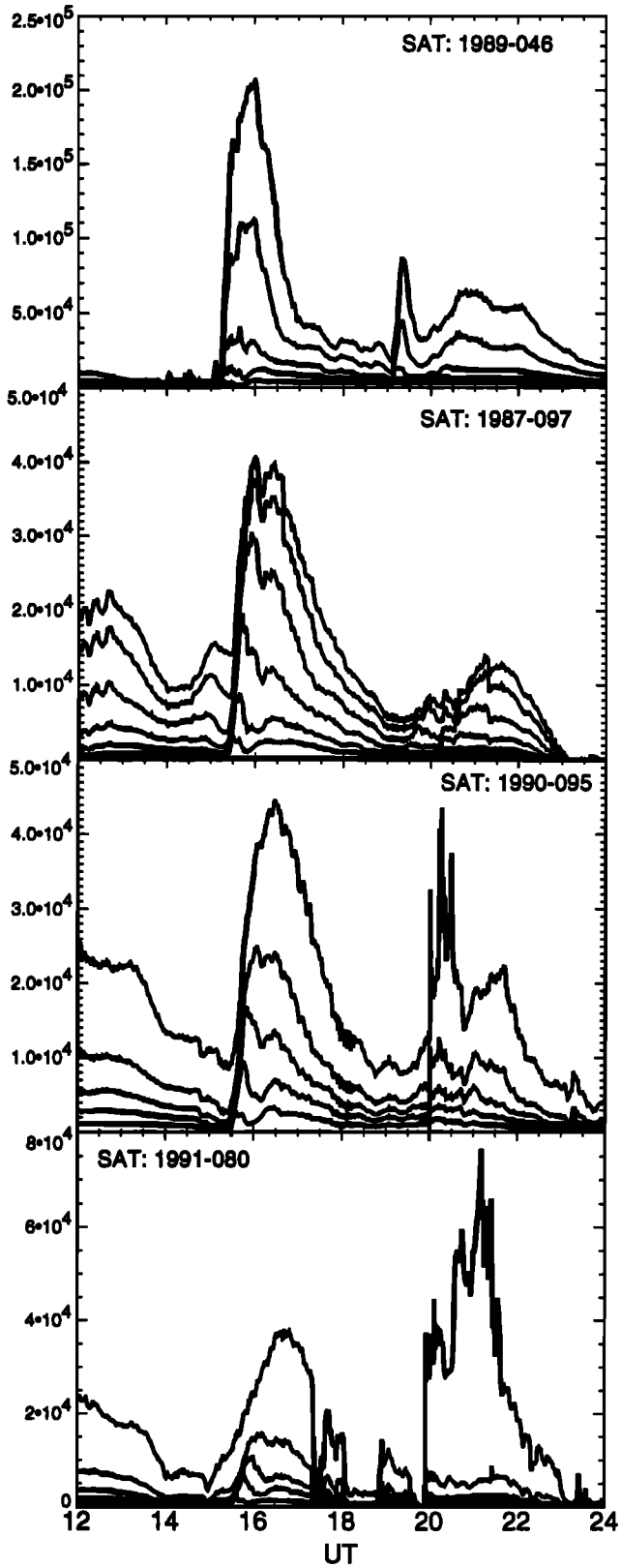


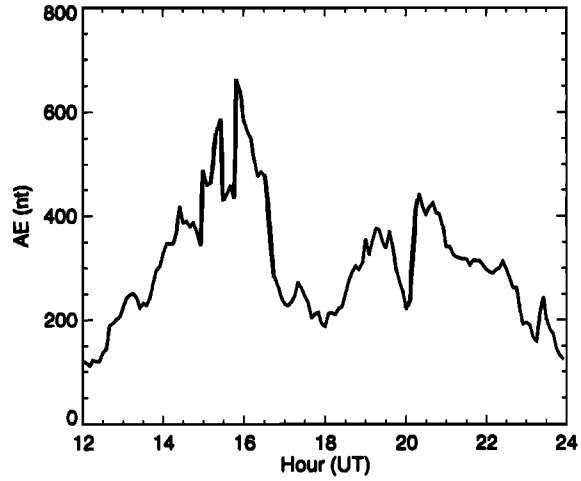


**Figure 13.** AE index for the period from 1200–1600 UT on March 29, 1992.

It is well known that the statistical location of the particle precipitation associated with the cusp shows a $B_y$ effect [*Candidi et al.*, 1983; *Newell et al.*, 1989]. These observations indicate that for $B_y$ negative (the conditions reported here), the cusp will be shifted toward the dawn side in the northern hemisphere. This is consistent with the fact that the observations reported here (1200–1600 UT) cover a period from about 0900–1300 MLT. At the same time as the cusp is shifted to the dawn side, however, the auroral oval itself is shifted to the dusk side [*Holzworth and Meng*, 1984], a fact which is incorporated into a number of ionospheric convection models [e.g., *Heppner and Maynard*, 1987; *Hairston and Heelis*, 1990]. The result is a tilt of the cusp with respect to the nominal L shells. For the $B_y < 0$ case, the tilt runs from the northwest to the southeast, in agreement with the observations shown in Figures 3 and 4. As the magnitude of $B_y$ increases, so will the tilt of the separatrix.

Although the results shown here are consistent with an IMF $B_y$ effect, the strong correlation between $B_x$ and $B_y$ (correlation coefficient 0.70) makes it impossible to rule out the possibility that the effect may be partly related to $B_x$. The weak correlation between the separatrix orientation and $B_z$ in comparison to the correlation with the other two

**Figure 12.** Electron flux data from the Los Alamos geosynchronous satellites, 1989-046, 1987-097, 1990-095, and 1991-080. The plot for satellite 1897-097 shows the summed energy channels 30–300 keV, 45–300 keV, 65–300 keV, 95–300 keV, 140–300 keV, and 200–300 keV. The plots for the other satellites show the summed energy channels 50–315 keV, 75–315 keV, 105–315 keV, 150–315 keV, and 225–315 keV. The data are averaged over approximately 1 min. The geographic longitudes of the satellites are (from top to bottom) −165.5°, −38.8°, +8.1°, and +70.4°.

components suggests that the $B_z$ control of the angle is negligible.

A model to explain the opposite shifts of the cusp and the auroral oval has been given by *Cowley et al.* [1991], in which the magnetic field within the ionosphere is treated as a dipole plus a uniform field due to the IMF-induced stresses at the magnetopause. An examination of their Figure 5 shows that there are really two IMF effects which would affect the cusp latitude: one is the shift due to the $y$ component and the other is a shift due to the $x$ component. In their example they used a magnitude of 6.5 nT for the $x/y$ field. If the field were purely in the $y$ direction the results from their Figure 5 indicate that the cusp would be at a latitude of about 74° at 1000 MLT and at 73.75° at 1100 MLT. This would lead to a boundary orientation of about −3°. If we were to add the effect of a negative $B_x$ of the same magnitude (6.5 nT) a slightly increased angle of about 4°–5° might result. However, in the case reported here, the actual value of $B_x$ is only about half the amount used by *Cowley et al.* [1991], so the expected magnitude of the effect should be less.

In contrast to the model proposed by *Cowley et al.* [1991], *Newell et al.* [1989] investigated the average latitude of the cusp for southward IMF on a statistical basis. In their Figure 4b, the average latitude of the cusp changes from just under 76° at 1100 MLT to just under 73° at 1130 MLT for the case when $B_x < -3$ nT (appropriate to the situation under discussion). This would lead to an angle of around −50° for the boundary orientation.

The observed results for this event show a much larger effect than predicted by *Cowley et al.* [1991], but they do not confirm the even larger effects observed by *Newell et al.* [1989] in their statistical results. The *Cowley et al.* [1991] model considers only the effects of IMF on the location of the open/closed boundary as a function of MLT and is clearly not a complete description of all the conditions that might affect the orientation of the separatrix. Modifications to include the effects of the distortion of the geomagnetic field due to other currents (for example the *DPY* currents) and the effects of a dawn–dusk asymmetry in the shape of the magnetopause may provide the additional effects necessary to explain the observed results. It is difficult to determine if the Cowley model is consistent with the variability of the boundary orientation observed here, since their paper does not give an explicit functional form for the position of the boundary as a function of $B_y$ and $B_x$, nor does it give a formula to describe the variation in the position of the separatrix as a function of IMF when all other conditions are kept constant.

## 5. Future Studies

The use of ground-based radar observations to monitor the polar cap potential would be a significant enhancement to our ability to monitor and eventually predict space weather. The technique described requires the determination of the orientation of the open/closed flux tube boundary, the motion of that boundary, and the plasma flow across the boundary. There is good agreement between the polar cap potential drops derived from the HF-radar data and the results derived using the AMIE technique on those occasions when the majority of the potential drop occurs over the 2–3 hours of MLT which lie within the radar field of view. However, since the ionospheric footprint of the merging line appears to often be of the order of 5 hours wide [*Crooker et al.*, 1991], the radar method often underestimates the total potential drop. The method could be considerably improved by using (1) higher time resolution data, here 5-min averages were used, which means that the effects of some FTEs might have been omitted; (2) two-dimensional vectors from the Super Dual Auroral Radar Network (SuperDARN) radars [*Greenwald et al.*, 1995], eliminating the assumptions concerning the uniformity of the flow required for a single radar; and (3) the complete SuperDARN chain of radars, which would cover a much larger range of magnetic local times and could observe the entire merging gap for much of the time. The full SuperDARN chain would also provide important information on the contribution of nightside reconnection to the cross-polar-cap potential.

The orientation of the ionospheric footprint of the merging line with respect to a constant magnetic latitude is closely related to the $y$ component of the IMF. The magnitudes observed are about an order of magnitude greater than predicted by *Cowley et al.* [1991]. The difference may be due to the effects of the *DPY* currents.

**Acknowledgments.** Support for the Goose Bay radar is provided in part by NSF grant ATM-9502993 and in part by NASA grant NAG5-1099. The studies of the relationship between the IMF and dayside convection patterns were also funded in part by NASA grant NAGW-2059 and NSF grant ATM-9111354. The study of conjugate phenomena is funded in part by NSF grant DPP-9421266. The authors are indebted to the Phillips Laboratory (AFSC), Department of the Air Force and B. Gill of the Frontec Corp., Canada, for their continuing support in the maintenance and operation of the Goose Bay radar at the Goose Bay Ionospheric Observatory. The authors are also indebted to R. P. Lepping for providing all the IMF data for the GEM campaign periods, to C. T. Russell for making the data easily available to the entire GEM community, and to G. Reeves at LANL for providing the geosynchronous satellite data from the LANL satellites. The authors also wish to thank all the participants of the GEM meetings, which have provided many helpful discussions and stimulating ideas. In particular, we thank L. R. Lyons and O. de la Beaujardière for their constant support and interest in the work reported here.

The Editor thanks two referees for their assistance in evaluating this paper.

## References

Baker, K.B., and S. Wing, A new magnetic coordinate system for conjugate studies at high latitudes, *J. Geophys. Res., 94,* 9139, 1989.

Baker, K.B., R.A. Greenwald, J.M. Ruohoniemi, J.R. Dudeney, M.J. Pinnock, N. Mattin, and J.M. Leonard, PACE—the Polar Anglo-American Conjugate Experiment, *EOS, 70,* 785 and 799, 1989.

Baker, K.B., R.A. Greenwald, J.M. Ruohoniemi, J.R. Dudeney, M. Pinnock, P.T. Newell, M.E. Greenspan, and C.-I. Meng, Simultaneous HF-radar and DMSP observations of the cusp, *Geophys. Res. Lett., 17,* 1869, 1990.

Baker, K.B., J.R. Dudeney, R.A. Greenwald, M. Pinnock, P.T. Newell, A.S. Rodger, and C.-I. Meng, HF-radar signatures of the cusp and the low-latitude boundary layer, *J. Geophys. Res., 100,* 7671, 1995.

Candidi, M., H.W. Kroehl, and C.-I. Meng, Intensity distribu-

tion of dayside polar soft electron precipitation and the IMF, *Planet. Space Sci., 31,* 489, 1983.

Clauer, C.R., and P.M. Banks, Relationship of the interplanetary electric field to the high-latitude ionospheric electric field and currents: Observations and model simulations, *J. Geophys. Res., 91,* 6959, 1986.

Cowley, S.W.H., J.P. Morelli, and M. Lockwood, Dependence of convective flows and particle precipitation in the high-latitude dayside ionosphere on the *X* and *Y* components of the interplanetary magnetic field, *J. Geophys. Res., 96,* 5557, 1991.

Crooker, N.U., Dayside merging and cusp geometry, *J. Geophys. Res., 84,* 951, 1979.

Crooker, N.U., F.R. Toffoletto, and M.S. Gussenhoven, Opening the cusp, *J. Geophys. Res., 96,* 3497, 1991.

de la Beaujardière, O., L.R. Lyons, and E. Friis-Christensen, Sondrestrom radar measurements of the reconnection electric field, *J. Geophys. Res., 96,* 13907, 1991.

Emery, B.A., et al., Electric potential patterns deduced for the SUNDIAL period of September 23-26, 1986, *Ann. Geophys., 8,* 399, 1990.

Etemadi, A., S.W.H. Cowley, M. Lockwood, B.J.I. Bromage, D.M. Willis, and H. Luhr, The dependence of high-latitude dayside ionospheric flows on the north-south component of the IMF: A high time resolution correlation analysis using EISCAT "Polar" and AMPTE UKS IRM data, *Planet. Space Sci., 36,* 471, 1988.

Freeman, M.P., J.M. Ruohoniemi, and R.A. Greenwald, The determination of time-stationary two-dimensional convection patterns with single station radars, *J. Geophys. Res., 96,* 15735, 1991.

Greenwald, R.A., K.B. Baker, R.A. Hutchins, and C. Hanuise, An HF phased-array radar for studying small-scale structure in the high-latitude ionosphere, *Radio Sci., 20,* 63, 1985.

Greenwald, R.A., K.B. Baker, J.M. Ruohoniemi, J.R. Dudeney, M. Pinnock, N. Mattin, J.M. Leonard, and R.P. Lepping, Simultaneous conjugate observations of dynamic variations in high-latitude dayside convection due to changes in IMF $B_y$, *J. Geophys. Res., 95,* 8057, 1990.

Greenwald, R.A., et al., DARN/SuperDARN: A global view of the dynamics of high-latitude convection, in *The Global Geospace Mission, Space Sci. Rev.,* vol. 71, edited by C. T. Russel, pp. 761–796, Kluwer Acad., Norwell, Mass., 1995.

Hairston, M.R., and R.A. Heelis, Model of the high-latitude ionospheric convection pattern during southward interplanetary magnetic field using DE 2 data, *J. Geophys. Res., 95,* 2333, 1990.

Heppner, J.P., and N.C. Maynard, Empirical high-latitude electric field models, *J. Geophys. Res., 92,* 4467, 1987.

Holzworth, R.H., and C.-I. Meng, Auroral boundary variations and the interplanetary magnetic field, *Planet. Space Sci., 32,* 25, 1984.

Knipp, D.J., A.D. Richmond, B. Emery, N.U. Crooker, O. dela Beaujardiere, D. Evans, and H. Kroehl, Ionospheric convection response to changing IMF direction, *Geophys. Res. Lett., 18,* 721, 1991.

Knipp, D.J., et al., Ionospheric convection response to slow, strong variations in a northward interplanetary magnetic field: A case study for January 14, 1988, *J. Geophys. Res., 98,* 19273, 1993.

Lester, M., M.P. Freeman, D.J. Southwood, J.A. Waldock, and H.J. Singer, A study of the relationship between interplanetary parameters and large displacements of the nightside polar cap boundary, *J. Geophys. Res., 95,* 21,133, 1990.

Lockwood, M., and C.J. Davis, On the longitude extent of magnetopause reconnection pulses, *Ann. Geophys.,* in press, 1997.

Lockwood, M., and M.F. Smith, Comment on "Mapping the dayside ionopshere to the magnetosphere according to particle precipitation characteristics" by Newell and Meng, *Geophys. Res. Lett., 20,* 1739, 1993.

Lockwood, M., S.W.H. Cowley, H. Todd, D.M. Willis, and C.R. Clauer, Ion flows and heating at a contracting polar-cap boundary, *Planet. Space Sci., 36,* 1229, 1988.

Lockwood, M., J. Moen, S.W.H. Cowley, A.D. Farmer, U.P. Løvhaug, H. Lühr, and V.N. Davda, Variability of dayside convection and motions of the cusp/cleft aurora, *Geophys. Res. Lett., 20,* 1011, 1993.

Lu, G., et al., Interhemispheric asymmetry of the high-latitude ionospheric convection pattern, *J. Geophys. Res., 99,* 6491, 1994.

Lu, G., et al., High-latitude ionospheric electrodynamics as determined by the AMIE procedure for the conjunctive SUNDIAL/ATLAS-1/GEM period of March 28-29, 1992, *J. Geophys. Res., 101,* 26,697, 1996.

Newell, P.T., and C.-I. Meng, The cusp and the cleft/boundary layer: Low-altitude identification and statistical local time variation, *J. Geophys. Res., 93,* 14,549, 1988.

Newell, P.T., and C.-I. Meng, Dipole tilt angle effects on the latitude of the cusp cleft/LLBL, *J. Geophys. Res., 94,* 6949, 1989.

Newell, P.T., and C.-I. Meng, Reply, *Geophys. Res. Lett., 20,* 1741, 1993.

Newell, P.T., and C.-I. Meng, Cusp low-energy ion cutoffs: A survey and implications for merging, *J. Geophys. Res., 100,* 21,943, 1995.

Newell, P.T., C.-I. Meng, D.G. Sibeck, and R.P. Lepping, Some low-altitude cusp dependencies on the interplanetary magnetic field, *J. Geophys. Res., 94,* 8921, 1989.

Pinnock, M., A.S. Rodger, J.R. Dudeney, F. Rich, and K.B. Baker, High spatial and temporal resolution observations of the ionospheric cusp, *Ann. Geophys., 13,* 919, 1995.

Richmond, A.D., Assimilative mapping of ionospheric electrodynamics, *Adv. Space Res., 12,* 59, 1992.

Richmond, A.D., and Y. Kamide, Mapping electrodynamic features of the high-latitude ionosphere from localized observations: Technique, *J. Geophys. Res., 93,* 5741, 1988.

Richmond, A.D., et al., Mapping electrodynamic features of the high-latitude ionosphere from localized observations: combined incoherent-scatter radar and magnetometer measurements for January 18–19, 1984, *J. Geophys. Res., 93,* 5760, 1988.

Rodger, A.S., S.B. Mende, T.J. Rosenberg, and K.B. Baker, Simultaneous optical and HF radar observations of the ionospheric cusp, *Geophys. Res. Lett., 22,* 2045, 1995.

Roelof, E.C., and D.G. Sibeck, Magnetopause shape as a bivariate function of interplanetary magnetic field $B_z$ and solar wind dynamic pressure, *J. Geophys. Res., 98,* 21,421, 1993.

Ruohoniemi, J.M., R.A. Greenwald, K.B. Baker, J.P. Villain, C. Hanuise, and J. Kelly, Mapping high-latitude plasma convection with coherent HF-radars, *J. Geophys. Res., 94,* 13,463, 1989.

Southwood, D.J., The ionospheric signature of flux transfer events, *J. Geophys. Res., 92,* 3207, 1987.

Szuszczewicz, E.P., et al., F-region climatology during the SUNDIAL/ATLAS-1 campaign of March 1992: Model-measurement comparisons and cause-effect relationships, *J. Geophys. Res., 101,* 26,741, 1996.

Todd, H., S.W.H. Cowley, M. Lockwood, and D.M. Willis, Response time of the high-latitude dayside ionosphere to

sudden changes in the north-south component of the IMF, *Planet. Space Sci., 36,* 1415, 1988.

Willis, D.M., M. Lockwood, S.W.H. Cowley, A.P. van Eyken, B.J.I. Bromage, H. Rishbeth, P.R. Smith, and S.R. Crothers, A survey of simultaneous observations of the high-latitude ionosphere and interplanetary magnetic field with EISCAT and AMPTE-UKS, *J. Atmos. Terr. Phys., 48,* 987, 1986.

K.B. Baker, Applied Physics Laboratory, The Johns Hopkins University, Johns Hopkins Road, Laurel, MD 20723-6099. (e-mail: kile_baker@jhuapl.edu)

G. Lu, High Altitude Observatory, National Center for Atmospheric Research, Boulder, CO 80397. (e-mail: ganglu@hao.ucar.edu)

A.S. Rodger, British Antarctic Survey, Madingley Road, Cambridge CB3 0ET, England. (e-mail: asro@pcmail.nerc-bas.ac.uk)

(Received October 8, 1996; revised December 10, 1996; accepted January 23, 1997.)